To be published in Applied Optics:

Title: Heterodyne photothermal spectroscopy of methane near 1651 nm inside hollow-core fiber using bismuth-doped fiber amplifier

Authors: Grzegorz Gomolka,Monika Krajewska,Aleksandr Khegai,Sergey Alyshev,Aleksey Lobanov,Sergey Firstov,Dariusz Pysz,Grzegorz Stepniewski,Ryszard Buczynski,Mariusz Klimczak,Michal Nikodem

Accepted: 13 April 21

Posted 14 April 21

DOI: https://doi.org/10.1364/AO.420044

Heterodyne photothermal spectroscopy of methane near 1651 nm inside hollow-core fiber using bismuth-doped fiber amplifier

GRZEGORZ GOMOLKA,[1,6] MONIKA KRAJEWSKA,[1,6] ALEKSANDR M. KHEGAI,[2] SERGEY V. ALYSHEV,[2] ALEKSEY S. LOBANOV,[3] SERGEI V. FIRSTOV,[2] DARIUSZ PYSZ,[4] GRZEGORZ STEPNIEWSKI,[4,5] RYSZARD BUCZYNSKI,[4,5] MARIUSZ KLIMCZAK,[5] AND MICHAL NIKODEM[1,*]

[1]*Department of Optics and Photonics, Wroclaw University of Science and Technology, Wybrzeze Wyspianskiego 27, 50-370 Wroclaw, Poland*
[2]*Prokhorov General Physics Institute of the Russian Academy of Sciences, Dianov Fiber Optics Research Center, 38 Vavilov str., 119333 Moscow, Russia*
[3]*Institute of Chemistry of High Purity Substances, Russian Academy of Sciences, 29 Tropinin str., 603600 Nizhny Novgorod, Russia*
[4]*Glass Department, Łukasiewicz Research Network - Institute of Microelectronics and Photonics, Al. Lotników 32/46, 02-668 Warsaw, Poland*
[5]*Faculty of Physics, University of Warsaw, Pasteura 5, 02-093 Warsaw, Poland*
[6]*These authors contributed equally to the presented work*
**michal.nikodem@pwr.edu.pl*

Abstract: In this paper we present laser-based methane detection near 1651 nm inside an anti-resonant hollow-core fiber (HCF) using photothermal spectroscopy (PTS). A bismuth-doped fiber amplifier capable of delivering up to more than 160 mW at 1651 nm is used to boost the PTS signal amplitude. The design of the system is described and the impact of various experimental parameters (such as pump source modulation frequency, modulation amplitude and optical power) on signal amplitude and signal to noise ratio is analyzed. Comparison with similar PTS/HCF-based systems is presented. With 1.3-m-long HCF and a fiber amplifier for signal enhancement this technique is capable of detecting methane at single parts-per-million (ppm) levels, which makes this robust in-fiber sensing approach promising also for industrial applications such as e.g. natural gas leak detection.

1. Introduction

Trace gas detection plays significant role in numerous applications, including industrial process control, environmental monitoring, security and medical diagnostics. Optical sensing, based on light-matter interaction principles, has proven excellent sensitivity, selectivity and stability not only in laboratories, but also in harsh environmental conditions. When combined with optical fibers, sensing systems become even more flexible, robust and immune to external disturbances, e.g. optical fibers enable simplifying the beam delivery from the source to the sensing cell [1] or allow for multi-point gas detection [2]. These configurations are particularly attractive in the near-infrared spectral region where components designed for telecom systems can be used and where numerous gases (such as methane [3,4], ethane [5], ammonia [6], hydrogen sulfide [7], and acetylene [8]) can be detected.

Another interesting possibility offered by optical fiber technology is to use optical fibers as gas cells for molecular detection. This can be accomplished with hollow-core fibers (HCFs) which have the ability to be filled with a gas sample. Various types of HCFs can be used for this purpose, including capillary fibers/waveguides with reflective inner coating, photonics band-gap (PBG) HCFs, or anti-resonant (AR) HCFs. Capillary fibers, due to

broadband transmission, are particularly attractive in the mid-infrared [9]. However, their integration with fiber-based near-infrared systems may not be straightforward. In this respect, silica-made PBG or AR HCFs have an advantage, e.g. they can be even spliced to standard single-mode fibers [10,11]. In the past two decades, the main focus was on PBG HCFs and numerous examples of using them for gas sensing have been demonstrated (e.g. [8,12–15]). However, more recently, the attention has shifted towards AR HCFs (often also referred as negative curvature HCFs) [16–19]. When used in gas detection, their main advantages are broad transmission bands (also in the mid-infrared [20,21]) and relatively large core size. The latter is beneficial when the fiber core has to be filled with gas: previous studies show filling times of less than 10 seconds when fiber lengths near 1 meter were used [22,23]. This is far shorter time than in the case of PBG HCFs where few minutes are typically reported [24,25].

The biggest drawback of using any kind of HCFs for gas sensing is the presence of interference fringes in the measured spectra. Typically, those fringes are due to the propagation of higher order spatial modes through the fiber. They may significantly reduce the detection limit of the system that retrieves information about the sample directly from the measurement of molecular absorption or molecular dispersion (using methods such as direct laser absorption spectroscopy, wavelength modulation spectroscopy or chirped laser dispersion spectroscopy). However, when techniques that rely on second-order effects are used (such as photothermal or photoacoustic spectroscopy), the impact of fringes is naturally reduced. For this reason photothermal spectroscopy (PTS; often also referred as photothermal interferometry or PTI) inside HCFs has been extensively studied by several groups, usually with very good performance. Typically, the HCF is placed in one arm of a Mach-Zehnder interferometer. The pump beam is used to produce density changes inside the HCF due to photothermal effect. These density changes (and, therefore, the refractive index changes) are detected as changes of the phase of the probe beam. The critical part of this approach is that one has to ensure that the interferometer operates at the quadrature. Therefore, a piezoelectric actuator is usually placed in the setup and its role is to control the length of the one arm of the interferometer. This configuration has been presented in multiple papers, e.g. in [26–29]. Some other examples of PTS-based sensing detect density changes using Fabry-Perot interferometer [30,31] or the interference between different spatial modes that propagate inside HCF [32,33].

So far, PTS-based near-infrared gas detection inside HCFs has been demonstrated primarily near 1.53 μm, using acetylene as target gas [26,27,30]. However, this approach can also be used with other molecules which have absorption lines in the near infrared spectral region. E.g. certain applications may benefit from using PTS and HCFs for methane (CH_4) detection: HCF-based sensing of methane in the near-infrared spectral region (typically near 1651 or 1653 nm) may be suitable for multi-point sensing applications, such as fugitive leak detection [34]. In this approach, the sensing nodes may be formed with multiple HCFs pieces that are connected with standard single-mode fiber [35,36]. Additionally, it was demonstrated that PTS has some unique properties, e.g. it enables simultaneous detection and localization of multiple, daisy-chained sensors [37]. Taking these into account, it seems that the main limitation for methane sensing in this configuration is the relatively low optical power that is available from laser diodes emitting near 1.65 μm (typically only a few milliwatts, seldomly slightly over ten milliwatts). This is particularly a problem in PTS, in which signal amplitude directly depends on optical power level [29,30]. In this work we address this issue by using a bismuth-doped fiber amplifier (BDFA) capable of delivering up to more than 160 mW when operating near 1651 nm. The main aim of this paper is to present photothermal spectroscopy of methane inside AR HCF. We demonstrate that using 1.3-m-long HCF and a fiber amplifier this technique is capable of detecting methane at parts-per-million (ppm) levels, with simple, fiber-to-fiber coupling only, and with no need for active mechanical stabilization of the

interferometer. Performance of the system is presented and technical challenges and limitations of the setup are discussed.

2. Experimental setup

The optical arrangement used for the heterodyne photothermal spectroscopy is schematically presented in Fig. 1. The proposed system works in the pump-probe configuration. The pump beam at 1651 nm is responsible for inducing the photothermal effect. The pump source comprises of a single-frequency distributed feedback (DFB) laser diode (from NTT Electronics) followed by an in-house developed BDFA. The laser diode is current modulated with a sinewave signal at f_m to enable phase-sensitive detection of the photothermal signal. Additionally, the laser current could be ramped in order to scan the emitted wavelength across the absorption line of methane. The BDFA is using bismuth-doped fiber made in the Dianov Fiber Optics Research Center and is capable of delivering up to ~160 mW of optical power at its output (more details can be found in [38]). The amplified light at 1651 nm is guided through an optical circulator into the 1.3-m-long silica-based HCF. The HCF has been made using the stack-and-draw technique in the Institute of Microelectronics and Photonics, Poland (an institute of the Łukasiewicz Research Network), it has an outer diameter of ~125 µm and core diameter of ~41 µm. Figure 2 shows the image of the HCF and its transmission bands in the visible and near-infrared spectral regions. The core of the HCF could be filled with a mixture of methane and air. The HCF is placed in one arm of the interferometer, which was used to detect the photothermal-induced density changes by measuring the changes of the phase of the probe beam. The probe source is a 1550 nm DFB laser diode with an output power of up to 20 mW. The probe beam is divided into two using a fiber coupler. The first beam is sent through the HCF, the second is frequency shifted by $f_a = 200$ MHz using an acousto-optical modulator (AOM; Fiber Q from Gooch&Housego). Both beams are subsequently combined using another fiber coupler and sent to a fast photodetector (model APD430C/M from Thorlabs) where they produced a heterodyne beatnote at f_a. In this sensing approach the phase changes due to photothermal effect could be detected as changes in the phase of the beatnote signal. In order to retrieve these phase changes, a fast lock-in amplifier is used (UHFLI from Zurich Instruments). Subsequently, the signal is demodulated at $2\times f_m$ which ensures that only signal from methane absorption will be measured.

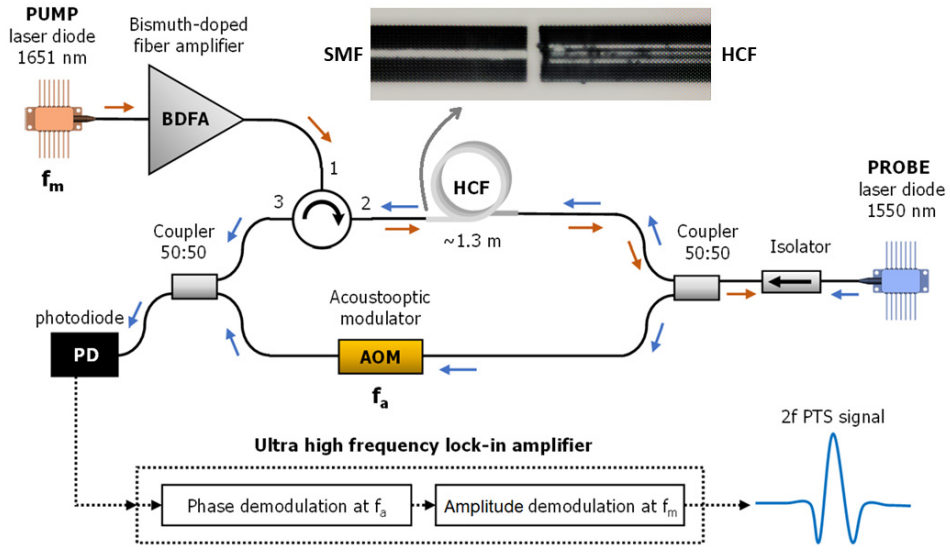

Fig. 1. Experimental setup used to perform heterodyne photothermal spectroscopy of methane at 1651 nm inside the anti-resonant hollow-core fiber.

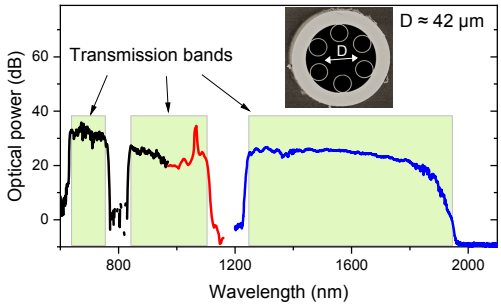

Fig. 2. The transmission bands of the HCF used in this work. For the measurement of the transmission bands light from a supercontinuum source (from Leukos) was coupled into the HCF and the optical spectrum was measured. Three spectrum analyzers were used to cover the whole spectrum: Ocean Optics Red Tide (up to 1000 nm; black line), Avantes Acaspec-nir256-1.7 (from 1000 nm to 1200 nm; red line) and OSA from Yokogawa (beyond 1200 nm; blue line). Inset shows the SEM image of the HCF.

The heterodyne-based detection of the photothermal signal was previously demonstrated in [39], where radio-frequency spectrum analyzer was used for beatnote signal demodulation. This approach has important advantage comparing to more common homodyne detection presented e.g. in [26]: it does not require the interferometer to be actively stabilized (in order to keep it in a quadrature point). The only requirement (that guarantees low noise level) is that the lengths of the two arms of the interferometer should be similar, which can be achieved without great effort. E.g. in our setup the lengths of the two arms were adjusted with fiber patchcords and the difference of ~5 cm was obtained. Additional advantage of using heterodyne detection is separation of pump and probe signals in the RF domain: even when some small part of the pump beam reaches the detector (e.g. due to some back-reflections), as long as it does not saturate the detector, it will have no impact on PTS measurement (because it is retrieved from the phase of the 200 MHz beatnote).

The light was coupled in and out of the HCF by aligning its both ends with standard single-mode fibers (SMFs) (as shown in the image in Fig. 1). Small (~10 µm) gaps were left between the HCF and SMFs. In this configuration the light coupling efficiency from SMF to HCF of more than ~35% could be typically obtained (dependence of coupling efficiency on the gap length is shown in Fig. 3). The transmission from HCF to SMF was lower, usually near 10%.

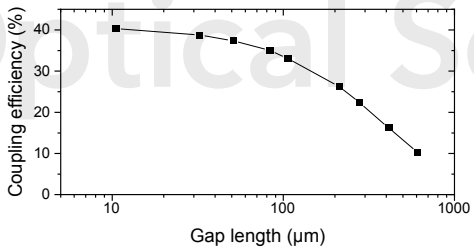

Fig. 3. The dependence of the coupling efficiency from SMF to HCF on the length of the gap between fibers.

3. Direct absorption spectroscopy

The HCF could be filled with a methane sample by applying a small (0.1 to 0.2 bar) pressure difference between its two ends. The filling times of only few seconds were observed which is a similar value to reported previously for AR HCFs with the same or similar length [23,40,41]. After the HCF was filled, the sample was kept at ambient pressure, the setup was aligned the exact concentration of methane could be determined based on the direct

absorption measurements and the HITRAN database [42]. In order to record direct absorption spectrum the laser current was modulated with a saw-tooth signal and the optical power was measured using the photodetector (placed between the fiber coupler and the isolator). Figure 4(a) shows the signal at the output of the photodetector measured as the source was wavelength-scanned across the methane transition (indicated with an arrow). The R(4) line near 1651 nm was selected because it is not only the strongest transition in the $2\nu_3$ methane absorption band, but it also has minimal interference from absorption lines of other molecules such as water vapor or carbon dioxide. After subtracting the baseline the absorption spectrum was obtained. It is presented in Fig. 4(b), together with a spectrum simulated using HITRAN database for methane in air with CH_4 concentration of 125 ppm. Although the absorption line is clearly visible, there are also optical fringes present in the background, which most likely are due to interference between the fundamental and higher-order modes propagating in the HCF.

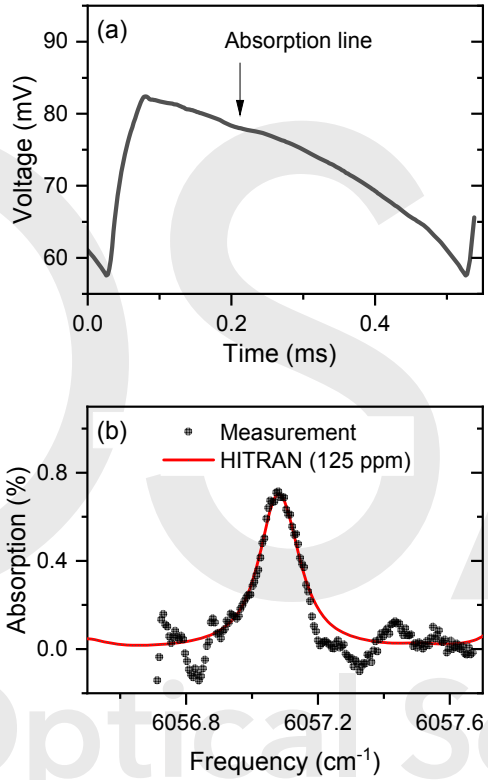

Fig. 4. (a) The signal at the output of the photodetector measured as the 1651-nm source was scanned across the methane transition; (b) absorption spectrum after baseline subtraction ('Measurement' plot) and HITRAN-based absorption spectrum of methane near 1651 nm.

4. Photothermal spectroscopy

4.1. System optimization

In PTS, two experimental parameters related to sinusoidal wavelength modulation of the pump beam had to be optimized: modulation amplitude and modulation frequency. Optimal modulation amplitude (that results in the highest PTS signal) depends on the width of the absorption line and is typically found experimentally (e.g. [31]). Figure 5 shows how PTS signal amplitude changes with modulation amplitude in our setup. Sample PTS spectrum is also presented in the inset. The signals were recorded at f_m = 2.5 kHz and for optical power of ~35 mW (inside HCF). The wavelength modulation was obtained through modulation of the

laser current with amplitudes from 10 mA to 30 mA (peak-to-peak). The optimum value was found to be near 20 mA which corresponds to a modulation amplitude of ~8 GHz (approximately 0.27 cm^{-1}). Good agreement between the measurement and simulation (model) based on the HITRAN database is obtained.

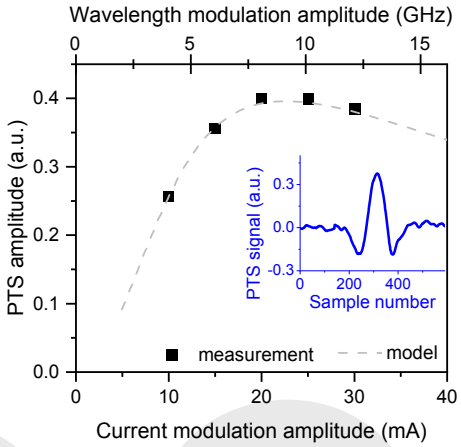

Fig. 5. PTS signal amplitude vs. current/wavelength modulation amplitude (of the pump source). PTS spectrum measured for modulation amplitude of 20 mA (corresponds to wavelength modulation amplitude of approximately 8 GHz) is shown in the inset.

The other critical parameter for PTS is how fast the wavelength of the pump beam is modulated. This issue was discussed in details in [30] where gas-filled HCF was analyzed using simplified model, in which HCF was considered as a capillary that guides only fundamental mode (with intensity profile described with a Gaussian function). According to these studies (which rely on earlier work presented in [43]), the PTS signal amplitude behaves like a single-pole function: it does not change with the modulation frequency up to a certain roll-off frequency f_0, and it drops as the modulation frequency goes beyond f_0. The main reason for this behavior is that at some point modulation of the gas temperature (which we observe as phase modulation of the probe beam) is not able to follow modulation of the pump beam and the system acts like a low-pass filter. As demonstrated in [30] the roll-off frequency of this filter depends on the mode field diameter of the pump beam: smaller diameter leads to larger roll-off frequency, which can reach few kilohertz for AR HCFs (with a core diameter of tens of μm) [28,29] or even tens of kilohertz for PBG HCFs (with a core diameter of less than 10 μm) [26].

Figure 6(a) shows how PTS amplitude depends on modulation frequency f_m in our setup. For frequencies up to few kilohertz the PTS amplitude is relatively constant but it drops when f_m larger than 5 kHz is used. This agrees well with the model and data presented in [30] (shown with line in Fig. 6(a)).

Additionally, we have analyzed how modulation frequency affects noise and SNR. These data are shown in Fig. 6(b) and 6(c), respectively. The noise was measured as the standard deviation of the signal amplitude, recorded when the wavelength of the pump source was adjusted to the center of the absorption line. As shown in Fig. 6(b), the noise drops when the modulation frequency increases. This can be explained by simple assumption that noise comes from two main sources: mechanical vibrations, which are particularly strong for frequencies below 1 kHz, and phase noise of the probe beam source, which for frequencies larger than kilohertz may be considered as constant [44]. As a result, there is a certain modulation frequency for which SNR reaches maximum (which again agrees well with the work of others [28,29]). In the case of our setup, the optimal value of f_m was found to be near 2.5 kHz.

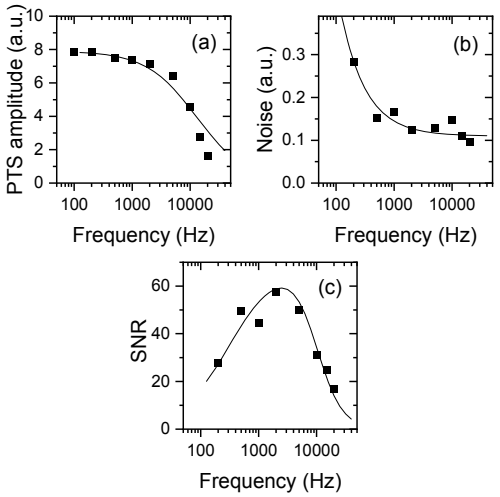

Fig. 6. Dependence of PTS amplitude (a), noise (b) and SNR (c) on modulation frequency f_m. Squares show actual measurement, line shows model (see text and [30] for details).

4.2. Performance evaluation

For the detection limit estimation the HCF was filled with methane/air mixture. The methane concentration of 125 ppm was determined based on direct absorption spectroscopy and data from the HITRAN database (as described in section 2). Subsequently, the signal amplitude dependence on pump power was analyzed. As mentioned earlier, the fiber amplifier was used in the setup. This possibility of PTS signal enhancement has been previously demonstrated in other spectral regions where more common fiber amplifiers are available (e.g. at 2 µm using thulium-doped fiber amplifier), but not at 1651 nm, where optical amplification is challenging. Figure 7(a) shows PTS spectra for four different pump powers. A linear dependence between the optical power and PTS amplitude is obtained, as shown in Fig. 7(b). It is also demonstrated that noise level does not depends on pump power level.

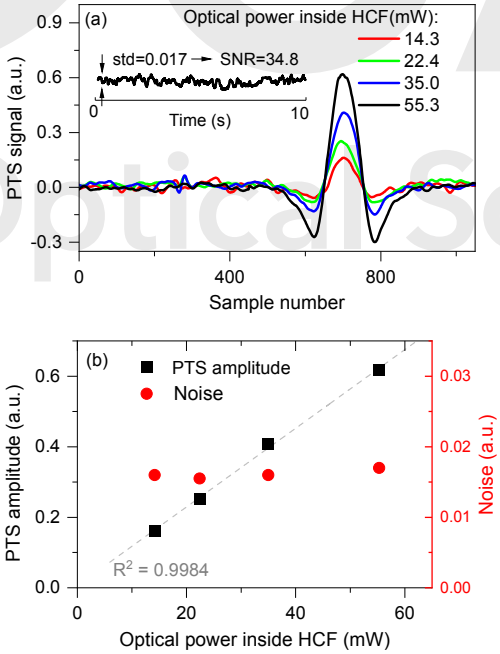

Fig. 7. (a) PTS spectra for 125 ppm methane measured at different pump powers (data points correspond to the wavelength, as the pump source was wavelength-scanned during the measurement). The inset shows data recorded after the pump source wavelength was adjusted to the center of the methane line; (b) PTS signal amplitude and noise vs. pump power.

For the highest available pump power (158 mW at the output of the BDFA, which corresponds to approximately 55 mW inside HCF) the SNR of ~34.8 was obtained, where the noise was calculated as the standard deviation of the signal amplitude recorded continuously for 10 seconds, after the wavelength of the pump source was adjusted to the transition center. Based on this SNR, the detection limit of 3.6 ppm can be calculated. Because the detection bandwidth was 3.124 Hz, this corresponds to bandwidth normalized concentration of ~2.04 ppm $Hz^{-1/2}$ and noise equivalent absorption coefficient (NEA) of 9.5×10^{-7} cm^{-1} $Hz^{-1/2}$.

5. Discussion

The setup presented in this paper is, to our best knowledge, the first ever example of methane detection inside a HCF using photothermal spectroscopy/interferometry. This method is particularly well-suited for HCF-based sensing because it is less affected by the optical fringes than standard methods which measure absorption directly. This is clearly visible when baseline in direct absorption measurement (Fig. 4) and PTS measurement (Fig. 7) are compared, both performed for the same gas sample. We can also compare the detection limit obtained in this work with the setup reported in [23], where WMS (wavelength modulation spectroscopy) technique was used near 3.3μm and performance was limited by optical fringes. Despite the fact, that the setup presented in that work was targeting the mid-infrared transition (almost two orders of magnitude stronger than absorption lines in the near-infrared) the detection limit was similar to presented here for PTS at ~1651 nm.

As we have pointed out across this work, PTS inside HCFs has been presented several times in the last few years, using different HCF types and different target molecules. The unique feature of the setup described in this paper is that it uses heterodyne-based detection which does not require interferometer to be stabilized at its quadrature point. Moreover, with a fast lock-in amplifier used for phase demodulation, the PTS signal is retrieved more efficiently compared to the configuration demonstrated previously in [39], where radio frequency spectrum analyzer was used. Furthermore, in order to boost the PTS signal amplitude, the system was combined with an in-house developed bismuth-doped fiber amplifier. As a result, the detection limit at the single-digit ppm level was obtained using only 1.3-m-long HCF.

Despite its simplicity (no need for interferometer stabilization), the setup presented in this paper reached the noise equivalent absorption coefficient comparable with some other PTS/AR HCF-based sensors. In particular, in [28] and [29], NEA of 4×10^{-5} cm^{-1} $Hz^{-1/2}$ (carbon dioxide detection near 2.3 μm, with 1.1 mW of optical power) and 2.5×10^{-6} cm^{-1} $Hz^{-1/2}$ (formaldehyde sensing near 3.6 μm, with 1.6 mW of optical power) were obtained, respectively. However, in both these cases active stabilization of the interferometer had to be implemented. Another example was published even more recently and can be found in [31]: ethane detection near 3.35 μm was demonstrated with novel interferometer design and NEA of 8.15×10^{-7} cm^{-1} (for 1-s integration time) was obtained.

Many sensing systems that target methane transitions near 1651 nm or 1653 nm can be found in the literature. In Table 1 we have listed the performance of some of them. In [45] a minimum detection limit of 11 ppm was obtained for the path length of 20 cm. Similar result was demonstrated in [46] where limit of detection of 29.5 ppm was obtained using a fiber-coupled open-path probe with a path-length of 40 m. Much lower detection limits was demonstrated when multi-pass cells were used for absorption signal enhancement. For example, 12 ppb was reported in [47] using path length of 290 m, which corresponds to ~3.5 ppm when normalized to the path length of 1 m. Similar performance was also reported in [3]

where dense multi-pass cell with the path length of 26.4 m was used and limit of detection of 79 ppb was obtained (which corresponds to ~2 ppm when normalized to the path length of 1 m). These results (all obtained using WMS technique) are similar to the performance of the setup presented in this work (detection limit of 2.06 ppm in 1 Hz for 1.3 m path length, corresponds to 2.68 ppm when normalized to the path length of 1 m). Moreover, comparing to methane sensors based on PBG-HCFs, the setup presented in this paper offers detection limit better than most of them (e.g. [12,48]). Similar performance was demonstrated only in [49] (4.3 ppm using 45-cm-long HCF) but it required more complex free-space coupling setup than presented in this paper.

Table 1. Performance comparison of several reported methane sensor systems and the reported setup.

Configuration	Detection limit (DL)	Path length (PL) [m]	DL×PL [ppm×m]
Single-pass [45]	11 ppm	0.2	2.2
Dual-pass, open-path [46]	29.5 ppm (for averaging time of 1 s)	0.4	11.8
Multi-pass [47]	12 ppb (for averaging time of 1 s)	290	3.48
Multi-pass [3]	79 ppb (for averaging time of 1 s)	26.4	2.09
PBG-HCF [12]	10 ppm	5.1	51
PBG-HCF [47]	10 ppm (for averaging time of 1 s)	0.8	8
PBG-HCF [49]	4.3 ppm (for averaging time of 0.5 s)	0.45	1.94
This work (AR-HCF)	2.06 ppm (for 1 Hz bandwidth)	1.3	2.68

The main technical limitations/challenges of the presented setup are related to light coupling in/out of the HCF and to heterodyne-signal phase demodulation using lock-in amplifier. Because the signal amplitude in PTS directly depends on pump power it is critical to couple as much of the pump beam into the HCF as possible. Furthermore, any optical power fluctuations will directly affect signal amplitude which will also require frequent calibration. Coupling efficiency can be improved using more sophisticated optical setup, e.g. efficiency of light coupling into AR HCF as high as 80% has been demonstrated in [50] with some bulk optics elements like mirrors and lenses. Another possibility is to permanently splice the HCF to standard solid-core fiber. The advantage of this approach is that it would additionally improve the robustness of the setup and address the stability issue. Recently it has been demonstrated that AR-HCF similar to one used in this work can be spliced to conventional fiber with losses as low as 2 dB [51]. In this scenario side-holes may be drilled in the HCF so that gas sample can still enter and leave the hollow core of the fiber [52,53].

The other issue is related to signal demodulation with the high-speed lock-in amplifier, which is used to detect and demodulate the phase of the heterodyne beatnote. Although we are only interested in its $2\times f_m$ component, the measured phase also has baseline which drifts (due to mechanical drifts of the setup) and, from time to time, jumps by $2\times\pi$. And anytime such a phase jump occurs (which in our experiments was from few times per second when the setup was disturbed to only once every few seconds during undisturbed operation) a spike is present in the PTS signal. It is important to point out that this issue is not related to the heterodyne-based PTS detection method itself, it only depends on how the demodulation process is performed e.g. it was not observed when radio frequency analyzer was used for signal demodulation [39]. For the setup presented here, if the long-term continuous operation of the sensor is needed, several options are possible. The simplest is to simultaneously observe the phase of the beatnote and remove unwanted data points (which account for only a few percent of total data points acquired). This can be done in real-time or during post-processing. A more advanced option would be to monitor the phase signal and, anytime it gets close to the $2\times\pi$ jump, correct the phase of the local oscillator. This approach would serve as a software-based equivalent of the mechanical stabilization of the interferometer that

was presented in many of the PTS-based sensors. Another solution that does not require mechanical modifications of the setup is to track the phase signal and use it as a feedback that controls the wavelength of the probe beam, as demonstrated recently in [31].

6. Conclusions

In conclusion, we have demonstrated photothermal spectroscopy of methane inside an anti-resonant hollow-core fiber. A detection limit of ~3.6 ppm was obtained using 1.3-m long fiber, corresponding to the minimum detectable absorption coefficient just below 10^{-6} cm^{-1} $Hz^{-1/2}$. This performance was obtained using near-infrared transitions, which makes the system compatible with standard fiber-based components. Additional signal enhancement was achieved by using a bismuth-doped fiber amplifier. We believe that similar sensing configurations, in which AR HCFs are used for methane detection near 1651 nm, may be very beneficial in applications such as fugitive methane leak detection and pipeline monitoring.

Funding. The National Science Centre, Poland, (UMO-2018/29/B/ST7/01730); The Ministry of Education and Science, Poland, 'Diamentowy Grant' (DI2019 0026 49); Russian Science Foundation (19-72-10003; with respect to Bi-doped fiber); Foundation for Polish Science, First TEAM programme co-financed by the European Union under the European Regional Development Fund (First TEAM/2016-1/1, POIR.04.04.00-00-1D64/16-00).

Acknowledgments. Department of Optics and Photonics (Wroclaw University of Science and Technology) acknowledges the financial support within the National Laboratory for Photonics and Quantum Technologies (NLPQT) infrastructural project (POIR.04.02.00-00-B003/18), co-financed by the European Regional Development Fund (ERDF).

Disclosures. The authors declare no conflicts of interest.

Data availability. Data underlying the results presented in this paper are available from the corresponding author upon reasonable request by email.

References

1. R. I. Woodward, M. R. Majewski, D. D. Hudson, and S. D. Jackson, "Swept-wavelength mid-infrared fiber laser for real-time ammonia gas sensing," APL Photonics **4**(2), 20801 (2019).
2. H. B. Yu, W. Jin, H. L. Ho, K. C. Chan, C. C. Chan, M. S. Demokan, G. Stewart, B. Culshaw, and Y. B. Liao, "Multiplexing of optical fiber gas sensors with a frequency-modulated continuous-wave technique," Appl. Opt. **40**(7), 1011–1020 (2001).
3. K. Liu, L. Wang, T. Tan, G. Wang, W. Zhang, W. Chen, and X. Gao, "Highly sensitive detection of methane by near-infrared laser absorption spectroscopy using a compact dense-pattern multipass cell," Sensors Actuators B Chem. **220**, 1000–1005 (2015).
4. T. Milde, M. Hoppe, H. Tatenguem, C. Assmann, W. Schade, and J. Sacher, "Comparison of the spectral excitation behavior of methane according to InP, GaSb, IC, and QC lasers as excitation source by sensor applications," Appl. Opt. **58**(10), C84–C91 (2019).
5. J. Jiang, Z. Wang, X. Han, C. Zhang, G. Ma, C. Li, and Y. Luo, "Multi-gas detection in power transformer oil based on tunable diode laser absorption spectrum," IEEE Trans. Dielectr. Electr. Insul. **26**(1), 153–161 (2019).
6. M. E. Webber, M. Pushkarsky, and C. K. N. Patel, "Fiber-amplifier-enhanced photoacoustic spectroscopy with near-infrared tunable diode lasers," Appl. Opt. **42**(12), 2119–2126 (2003).
7. H. Wu, L. Dong, X. Liu, H. Zheng, X. Yin, W. Ma, L. Zhang, W. Yin, and S. Jia, "Fiber-Amplifier-Enhanced QEPAS Sensor for Simultaneous Trace Gas Detection of NH_3 and H_2S," Sensors **15**(10), 26743–26755 (2015).
8. T. Ritari, J. Tuominen, H. Ludvigsen, J. C. Petersen, T. Sørensen, T. P. Hansen, and H. R. Simonsen, "Gas sensing using air-guiding photonic bandgap fibers," Opt. Express **12**(17), 4080–4087 (2004).
9. D. Francis, J. Hodgkinson, B. Livingstone, P. Black, and R. P. Tatam, "Low-volume, fast response-time hollow silica waveguide gas cells for mid-IR spectroscopy," Appl. Opt. **55**(25), 6797–6806 (2016).
10. K. Z. Aghaie, M. J. F. Digonnet, and S. Fan, "Optimization of the splice loss between photonic-bandgap fibers and conventional single-mode fibers," Opt. Lett. **35**(12), 1938–1940 (2010).
11. S. Gao, Y. Wang, C. Tian, and P. Wang, "Splice Loss Optimization of a Photonic Bandgap Fiber via a High V-Number Fiber," IEEE Photonics Technol. Lett. **26**(21), 2134–2137 (2014).
12. A. M. Cubillas, M. Silva-Lopez, J. M. Lazaro, O. M. Conde, M. N. Petrovich, and J. M. Lopez-Higuera, "Methane detection at 1670-nm band using a hollow-core photonic bandgap fiber and a multiline algorithm," Opt. Express **15**(26), 17570–17576 (2007).
13. N. Gayraud, Ł. W. Kornaszewski, J. M. Stone, J. C. Knight, D. T. Reid, D. P. Hand, and W. N. MacPherson, "Mid-infrared gas sensing using a photonic bandgap fiber," Appl. Opt. **47**(9), 1269–1277

(2008).
14. J. P. Parry, B. C. Griffiths, N. Gayraud, E. D. McNaghten, A. M. Parkes, W. N. MacPherson, and D. P. Hand, "Towards practical gas sensing with micro-structured fibres," Meas. Sci. Technol. **20**(7), 75301 (2009).
15. Y. Wang, G. Ma, D. Zheng, W. Liao, J. Jiang, and W. Qin, "Detection of Dissolved Acetylene in Power Transformer Oil Based on Photonic Crystal Fiber," IEEE Sens. J. **20**(18), 10981–10988 (2020).
16. F. Yu and J. C. Knight, "Negative Curvature Hollow-Core Optical Fiber," IEEE J. Sel. Top. Quantum Electron. **22**(2), 146–155 (2016).
17. C. Wei, R. J. Weiblen, C. R. Menyuk, and J. Hu, "Negative curvature fibers," Adv. Opt. Photon. **9**(3), 504–561 (2017).
18. B. Debord, F. Amrani, L. Vincetti, F. Gérôme, and F. Benabid, "Hollow-Core Fiber Technology: The Rising of "Gas Photonics,"" Fibers **7**(2), 16 (2019).
19. G. T. Jasion, J. R. Hayes, N. V Wheeler, Y. Chen, T. D. Bradley, D. J. Richardson, and F. Poletti, "Fabrication of tubular anti-resonant hollow core fibers: modelling, draw dynamics and process optimization," Opt. Express **27**(15), 20567–20582 (2019).
20. A. D. Pryamikov, A. S. Biriukov, A. F. Kosolapov, V. G. Plotnichenko, S. L. Semjonov, and E. M. Dianov, "Demonstration of a waveguide regime for a silica hollow - core microstructured optical fiber with a negative curvature of the core boundary in the spectral region > 3.5 μm," Opt. Express **19**(2), 1441–1448 (2011).
21. M. Klimczak, D. Dobrakowski, A. N. Ghosh, G. Stępniewski, D. Pysz, G. Huss, T. Sylvestre, and R. Buczyński, "Nested capillary anti-resonant silica fiber with mid-infrared transmission and low bending sensitivity at 4000 nm," Opt. Lett. **44**(17), 4395–4398 (2019).
22. C. Yao, L. Xiao, S. Gao, Y. Wang, P. Wang, R. Kan, W. Jin, and W. Ren, "Sub-ppm CO detection in a sub-meter-long hollow-core negative curvature fiber using absorption spectroscopy at 2.3 μm," Sensors Actuators B Chem. **303**, 127238 (2020).
23. M. Nikodem, K. Krzempek, G. Dudzik, and K. Abramski, "Hollow core fiber-assisted absorption spectroscopy of methane at 3.4 μm," Opt. Express **26**(17), 21843–21848 (2018).
24. S. M. Mejia Quintero, L. C. Guedes Valente, M. S. De Paula Gomes, H. da Silva, B. de Souza, and S. R. K. Morikawa, "All-Fiber CO_2 Sensor Using Hollow Core PCF Operating in the 2 μm Region," Sensors **18**(12), 4393 (2018).
25. P. Jaworski, "Molecular dispersion spectroscopy in a CO_2-filled all-fiber gas cells based on a hollow-core photonic crystal fiber," Opt. Eng. **58**(2), 1–8 (2019).
26. W. Jin, Y. Cao, F. Yang, and H. L. Ho, "Ultra-sensitive all-fibre photothermal spectroscopy with large dynamic range," Nat. Commun. **6**, 6767 (2015).
27. Y. Lin, W. Jin, F. Yang, J. Ma, C. Wang, H. L. Ho, and Y. Liu, "Pulsed photothermal interferometry for spectroscopic gas detection with hollow-core optical fibre," Sci. Rep. **6**(1), 39410 (2016).
28. C. Yao, Q. Wang, Y. Lin, W. Jin, L. Xiao, S. Gao, Y. Wang, P. Wang, and W. Ren, "Photothermal CO detection in a hollow-core negative curvature fiber," Opt. Lett. **44**(16), 4048–4051 (2019).
29. C. Yao, S. Gao, Y. Wang, P. Wang, W. Jin, and W. Ren, "MIR-Pump NIR-Probe Fiber-Optic Photothermal Spectroscopy With Background-Free First Harmonic Detection," IEEE Sens. J. **20**(21), 12709–12715 (2020).
30. H. Bao, Y. Hong, W. Jin, H. L. Ho, C. Wang, S. Gao, Y. Wang, and P. Wang, "Modeling and performance evaluation of in-line Fabry-Perot photothermal gas sensors with hollow-core optical fibers," Opt. Express **28**(4), 5423–5435 (2020).
31. F. Chen, S. Jiang, W. Jin, H. Bao, H. L. Ho, C. Wang, and S. Gao, "Ethane detection with mid-infrared hollow-core fiber photothermal spectroscopy," Opt. Express **28**(25), 38115–38126 (2020).
32. P. Zhao, Y. Zhao, H. Bao, H. L. Ho, W. Jin, S. Fan, S. Gao, Y. Wang, and P. Wang, "Mode-phase-difference photothermal spectroscopy for gas detection with an anti-resonant hollow-core optical fiber," Nat. Commun. **11**(1), 847 (2020).
33. P. Zhao, H. L. Ho, W. Jin, S. Fan, S. Gao, Y. Wang, and P. Wang, "Gas sensing with mode-phase-difference photothermal spectroscopy assisted by a long period grating in a dual-mode negative-curvature hollow-core optical fiber," Opt. Lett. **45**(20), 5660–5663 (2020).
34. J. Karp, W. Challener, M. Kasten, N. Choudhury, S. Palit, G. Pickrell, D. Homa, A. Floyd, Y. Cheng, F. Yu, and J. Knight, "Fugitive methane leak detection using mid-infrared hollow-core photonic crystal fiber containing ultrafast laser drilled side-holes," in *Fiber Optic Sensors and Applications XIII*, E. Udd, G. Pickrell, and H. H. Du, eds. (SPIE, 2016), **9852**, pp. 259–265.
35. Y. Lin, F. Liu, X. He, W. Jin, M. Zhang, F. Yang, H. L. Ho, Y. Tan, and L. Gu, "Distributed gas sensing with optical fibre photothermal interferometry," Opt. Express **25**(25), 31568–31585 (2017).
36. W. A. Challener, M. A. Kasten, J. Karp, and N. Choudhury, "Hollow-core fiber sensing technique for pipeline leak detection," in *Photonic Instrumentation Engineering V*, Y. G. Soskind, ed. (SPIE, 2018), **10539**, pp. 143–152.
37. M. Nikodem and G. Wysocki, "Localized Chemical Detection in Quasi-Distributed Multi-Node Fiber-Ring Network," J. Light. Technol. **36**(24), 5921–5926 (2018).
38. G. Gomółka, M. Krajewska, M. Kaleta, A. M. Khegai, S. V Alyshev, A. S. Lobanov, S. V Firstov, and M. Nikodem, "Operation of a Single-Frequency Bismuth-Doped Fiber Power Amplifier near 1.65 μm,"

Photonics **7**(4), 128 (2020).
39. K. Krzempek, G. Dudzik, K. Abramski, G. Wysocki, P. Jaworski, and M. Nikodem, "Heterodyne interferometric signal retrieval in photoacoustic spectroscopy," Opt. Express **26**(2), 1125–1132 (2018).
40. M. Nikodem, G. Gomółka, M. Klimczak, D. Pysz, and R. Buczyński, "Demonstration of mid-infrared gas sensing using an anti-resonant hollow core fiber and a quantum cascade laser," Opt. Express **27**(25), 36350–36357 (2019).
41. P. Jaworski, K. Krzempek, G. Dudzik, P. Sazio, and W. Belardi, "Nitrous Oxide detection at 5.26 μm with a compound glass Antiresonant Hollow-Core Optical Fiber," Opt. Lett. **45**(6), 1326–1329 (2020).
42. I. E. Gordon, L. S. Rothman, C. Hill, R. V Kochanov, Y. Tan, P. F. Bernath, M. Birk, V. Boudon, A. Campargue, K. V Chance, B. J. Drouin, J.-M. Flaud, R. R. Gamache, J. T. Hodges, D. Jacquemart, V. I. Perevalov, A. Perrin, K. P. Shine, M.-A. H. Smith, J. Tennyson, G. C. Toon, H. Tran, V. G. Tyuterev, A. Barbe, A. G. Császár, V. M. Devi, T. Furtenbacher, J. J. Harrison, J.-M. Hartmann, A. Jolly, T. J. Johnson, T. Karman, I. Kleiner, A. A. Kyuberis, J. Loos, O. M. Lyulin, S. T. Massie, S. N. Mikhailenko, N. Moazzen-Ahmadi, H. S. P. Müller, O. V Naumenko, A. V Nikitin, O. L. Polyansky, M. Rey, M. Rotger, S. W. Sharpe, K. Sung, E. Starikova, S. A. Tashkun, J. Vander Auwera, G. Wagner, J. Wilzewski, P. Wcisło, S. Yu, and E. J. Zak, "The HITRAN2016 molecular spectroscopic database," J. Quant. Spectrosc. Radiat. Transf. **203**, 3–69 (2017).
43. C. C. Davis and S. J. Petuchowski, "Phase fluctuation optical heterodyne spectroscopy of gases," Appl. Opt. **20**(14), 2539–2554 (1981).
44. K. Kikuchi, "Characterization of semiconductor-laser phase noise and estimation of bit-error rate performance with low-speed offline digital coherent receivers," Opt. Express **20**(5), 5291–5302 (2012).
45. C.-T. Zheng, J.-Q. Huang, W.-L. Ye, M. Lv, J.-M. Dang, T.-S. Cao, C. Chen, and Y.-D. Wang, "Demonstration of a portable near-infrared CH_4 detection sensor based on tunable diode laser absorption spectroscopy," Infrared Phys. Technol. **61**, 306–312 (2013).
46. B. Li, C. Zheng, H. Liu, Q. He, W. Ye, Y. Zhang, J. Pan, and Y. Wang, "Development and measurement of a near-infrared CH_4 detection system using 1.654μm wavelength-modulated diode laser and open reflective gas sensing probe," Sensors Actuators B Chem. **225**, 188–198 (2016).
47. J. Xia, F. Zhu, S. Zhang, A. Kolomenskii, and H. Schuessler, "A ppb level sensitive sensor for atmospheric methane detection," Infrared Phys. Technol. **86**, 194–201 (2017).
48. Q. He, P. Dang, Z. Liu, C. Zheng, and Y. Wang, "TDLAS–WMS based near-infrared methane sensor system using hollow-core photonic crystal fiber as gas-chamber," Opt. Quantum Electron. **49**(3), 115 (2017).
49. L. Hu, C. Zheng, D. Yao, D. Yu, Z. Liu, J. Zheng, Y. Wang, and F. K. Tittel, "A hollow-core photonic band-gap fiber based methane sensor system capable of reduced mode interference noise," Infrared Phys. Technol. **97**, 101–107 (2019).
50. X. Zhu, D. Wu, Y. Wang, F. Yu, Q. Li, Y. Qi, J. Knight, S. Chen, and L. Hu, "Delivery of CW laser power up to 300 watts at 1080 nm by an uncooled low-loss anti-resonant hollow-core fiber," Opt. Express **29**(2), 1492–1501 (2021).
51. M. Yucheng, A. Filipkowski, G. Stepniewski, D. Dobrakowski, J. Zhou, B. Lou, M. Klimczak, L. Zhao, and R. Buczynski, "Fusion splicing of silica hollow core anti-resonant fibers with polarization maintaining fibers," J. Light. Technol. doi: 10.1109/JLT.2021.3058888 (2021).
52. M. Hou, F. Zhu, Y. Wang, Y. Wang, C. Liao, S. Liu, and P. Lu, "Antiresonant reflecting guidance mechanism in hollow-core fiber for gas pressure sensing," Opt. Express **24**(24), 27890–27898 (2016).
53. C. C. Novo, D. Choudhury, B. Siwicki, R. R. Thomson, and J. D. Shephard, "Femtosecond laser machining of hollow-core negative curvature fibres," Opt. Express **28**(17), 25491–25501 (2020).